# CYCLOTRON HARMONIC WAVE PROPAGATION AND INSTABILITIES: I. PERPENDICULAR PROPAGATION

by

J. A. Tataronis and F. W. Crawford

NASA Research Grant NGR 05-020-077

and

AEC Contract AT(04-3)326
(Project Agreement No. 1)

SU-IPR Report No. 325

June 1969



Institute for Plasma Research
Stanford University
Stanford, California

# CYCLOTRON HARMONIC WAVE PROPAGATION AND INSTABILITIES: I. PERPENDICULAR PROPAGATION

by

J. A. Tataronis† and F. W. Crawford

Institute for Plasma Research

Stanford University

Stanford, California

## ABSTRACT

Parts I and II of this paper present a comprehensive picture of longitudinal wave propagation in a warm homogeneous magnetoplasma. Part I discusses computed dispersion characteristics for propagation perpendicular to the static magnetic field. For a ring electron velocity distribution it is found that mode coupling and absolute instability can occur. Similar effects are predicted for a spherical shell distribution. The Maxwellian distribution gives rise to stable propagation of undamped waves, and attenuating standing waves. A mixture of ring and Maxwellian distributions can give absolute instability with stronger growth and lower instability thresholds than for the ring distribution alone. Propagation oblique to the static magnetic field will be dealt with in Part II [SU-IPR Report No. 326].

PT. I - N.I.

† Now at CEN de Saclay, France

CONTENTS


| | | Page |
|---|---|---|
| | ABSTRACT | ii |
| 1. | INTRODUCTION | 1 |
| 2. | THEORY | 2 |
| | Dispersion Relation | 3 |
| | Stability Considerations | 4 |
| | Instability Classification | 5 |
| 3. | RING DISTRIBUTION | 9 |
| | Dispersion Characteristics | 9 |
| | Stability Analysis | 13 |
| 4. | SPHERICAL SHELL DISTRIBUTION | 15 |
| | Dispersion Characteristics | 16 |
| 5. | MAXWELLIAN DISTRIBUTION | 18 |
| | Dispersion Characteristics | 18 |
| | Collisional Effects | 22 |
| 6. | MIXED DISTRIBUTION | 24 |
| | Dispersion Characteristics | 24 |
| 7. | DISCUSSION | 28 |
| | REFERENCES | 29 |

LIST OF FIGURES


| | | Page |
|---|---|---|
| 1. | Deformation of contour of integration of (16) as $\omega$ approaches real axis from the Laplace contour. . . . . | 7 |
| 2. | Dispersion characteristics of perpendicularly propagating cyclotron harmonic waves: Ring distribution . . . . . | 10-11 |
| 3. | Application of instability criteria to perpendicularly propagating cyclotron harmonic waves | |
| | (a) Pinching pole criterion . . . . . | 14 |
| | (b) Frequency loop criterion . . . . . | 14 |
| 4. | Dispersion characteristics of perpendicularly propagating cyclotron harmonic waves: Spherical shell distribution . . . . . | 17 |
| 5. | Dispersion characteristics of perpendicularly propagating cyclotron harmonic waves: Maxwellian distribution ($k_\perp$ real) . . . . . | 19 |
| 6. | Dispersion characteristics of perpendicularly propagating cyclotron harmonic waves: Maxwellian distribution ($k_\perp$ complex). . . . . | 20 |
| 7. | Dispersion characteristics of perpendicularly propagating cyclotron harmonic waves: Maxwellian distribution with collisions . . . . . | 23 |
| 8. | Perpendicularly propagating cyclotron harmonic waves: Instability threshold for a mixture of ($\alpha$) Maxwellian and ($1-\alpha$) ring electron velocity distributions . . . . . | 25 |
| 9. | Perpendicularly propagating cyclotron harmonic waves: Maximum instability growth rates for a mixture of ($\alpha$) Maxwellian and ($1-\alpha$) ring electron velocity distributions. . . . . | 25 |

10. Dispersion characteristics of perpendicularly propagating cyclotron harmonic waves: Mixture of ($\alpha$) Maxwellian and (1-$\alpha$) ring electron velocity distribution . . . . . 27

# 1. INTRODUCTION

In 1958, Bernstein published a comprehensive paper summarizing the procedure for obtaining the dispersion relation for longitudinal waves in a warm homogeneous magnetoplasma, and describing some of their properties. Over the last ten years, well over a hundred papers have appeared, treating theoretical and experimental aspects of these waves. It is not our intention to review this material. That has been done elsewhere (Crawford 1968). We wish to present systematically in a single source the salient features emerging from study of the dispersion relation for a variety of electron velocity distributions. Many of the results are new. Others are scattered through the literature, and can benefit from inclusion in a coherent picture such as this paper aims to present. We shall stress numerical solutions of the very complicated expressions involved, rather than the mathematical formalism, and will interpret properties of the predicted propagation characteristics in the light of the refined stability criteria that have been developed in recent years (Derfler 1961, 1967, 1969; Briggs 1964).

The paper divides naturally into two parts. The first deals with propagation perpendicular to the magnetic field, for which collisionless cyclotron and Landau damping effects do not occur. Part II treats oblique propagation, for which they are important. In each case, similar procedure is followed. The dispersion relation for a given velocity distribution is first solved for complex frequency and real wavenumber, to establish whether instability is predicted. If so, stability criteria are applied to determine whether the instability is convective or absolute (Sturrock 1958). Finally, if absolute instability is absent, the dispersion relation is solved for real frequency and complex wavenumber.

The plan of Part I is as follows. Section 2 describes first the procedure for obtaining a dispersion relation, then comments on the conditions under which instabilities may be encountered, and finally presents the stability criteria used to classify them. Sections 3 to 6 analyze the propagation for specific electron velocity distributions. Section 7 provides a brief discussion of the results.

## 2. THEORY

The basic equations from which warm magnetoplasma propagation characteristics are derived in the quasistatic approximation are Poisson's equation and the linearized Vlasov equation (Stix 1962),

$$\nabla \cdot \underset{\sim}{E}(\underset{\sim}{r},t) = \frac{\rho_s(\underset{\sim}{r},t)}{\epsilon_0} - \frac{n_0 e}{\epsilon_0} \int d\underset{\sim}{v}\, f_1(\underset{\sim}{v},\underset{\sim}{r},t) \quad , \tag{1}$$

$$\frac{\partial f_1}{\partial t} + \underset{\sim}{v} \cdot \nabla f_1 - \frac{e}{m} \underset{\sim}{v} \times \underset{\sim}{B}_0 \cdot \frac{\partial f_1}{\partial \underset{\sim}{v}} = \frac{e}{m} \underset{\sim}{E} \cdot \frac{\partial f_0}{\partial \underset{\sim}{v}} \quad , \tag{2}$$

where the plasma is assumed uniform and infinite, with a time invariant electron velocity distribution, $f_0(v_\perp, v_\parallel)$; $v_\perp$ and $v_\parallel$ are the components of the electron velocity, $\underset{\sim}{v}$, perpendicular and parallel to the external magnetic field, $\underset{\sim}{B}_0$; $f_1$ is the lowest order term in the perturbation expansion of the electron velocity distribution; $\underset{\sim}{E}$ is the perturbation electric field; $\rho_s$ is the external charge density representing the source of the perturbations; $-e$ is the electron charge; $m$ is the electron mass; $n_0 (= n_{e0} = n_{i0})$ is the average charged particle density, and $\epsilon_0$ is the permittivity of free space. Ion motions will be neglected.

To solve (1) and (2), we introduce a Fourier transform in space, and a Laplace transform in time, defined with their inverse transformation as

$$\underset{\sim}{E}(\underset{\sim}{k},\omega) = \int_0^\infty dt \int d\underset{\sim}{r} \exp i(\underset{\sim}{k}\cdot\underset{\sim}{r} - \omega t)\underset{\sim}{E}(\underset{\sim}{r},t) \quad , \tag{3}$$

$$\underset{\sim}{E}(\underset{\sim}{r},t) = \int_C \frac{d\omega}{2\pi} \int \frac{d\underset{\sim}{k}}{(2\pi)^3} \exp i(\omega t - \underset{\sim}{k}\cdot\underset{\sim}{r})\underset{\sim}{E}(\underset{\sim}{k},\omega) \quad , \tag{4}$$

where $C$ is the Laplace contour in the lower half complex $\omega$-plane. Transforming (1) and (2), and combining, yields

$$E(k,\omega) = \frac{ik\rho_s(\underset{\sim}{k},\omega)}{\epsilon_0 k^2 K(\omega,\underset{\sim}{k})} \quad , \tag{5}$$

where $k^2 = k_\perp^2 + k_\parallel^2$ and the plasma equivalent permittivity is,

$$K(\omega,\underset{\sim}{k}) = 1 + \frac{\omega_p^2}{k^2} \sum_{n=-\infty}^{\infty} \int_{-\infty}^{\infty} dv_\parallel \frac{H_n(v_\parallel)}{\omega - k_\parallel v_\parallel - n\omega_c} \qquad (\omega_i < 0) \ ,$$

$$H_n(v_\parallel) = 2\pi \int_0^{\infty} dv_\perp \left( \frac{n\omega_c}{v_\perp} \frac{\partial f_0}{\partial v_\perp} + k_\parallel \frac{\partial f_0}{\partial v_\parallel} \right) J_n^2 \left( \frac{k_\perp v_\perp}{\omega_c} \right) v_\perp \ , \qquad (6)$$

where $k_\perp$ and $k_\parallel$ are the components of the wavevector, k, perpendicular and parallel to the applied magnetic field; $\omega_p \left( = n_0 e^2/\epsilon_0 m)^{\frac{1}{2}} \right)$ is the electron plasma frequency; $\omega_c (= eB_0/m)$ is the electron cyclotron frequency; $J_n$ is the nth order Bessel function of the first kind, and $\omega_i$ is the imaginary part of $\omega (= \omega_r + i\omega_i)$.

Equation (5) can be inverted with the aid of (4) to yield,

$$E(\underset{\sim}{r},t) = \int_C \frac{d\omega}{2\pi} \exp(i\omega t) \underset{\sim}{G}(\omega,\underset{\sim}{r}) \ ,$$

$$\underset{\sim}{G}(\omega,\underset{\sim}{r}) = \int \frac{d\underset{\sim}{k}}{(2\pi)^3} \frac{\exp(-i\underset{\sim}{k}\cdot\underset{\sim}{r}) \rho_s(\underset{\sim}{k},\omega) \underset{\sim}{k}}{\epsilon_0 k^2 K(\omega,\underset{\sim}{k})} \ . \qquad (7)$$

## Dispersion Relation

The dispersion relation is simply $K(\omega,\underset{\sim}{k}) = 0$, and describes the propagation of waves varying as $\exp i(\omega t - \underset{\sim}{k}\cdot\underset{\sim}{r})$. If we solve for $\omega(\underset{\sim}{k}$ real), exponential growth and decay are implied for $\omega_i < 0$ and $\omega_i > 0$, respectively, while $\omega_i = 0$ indicates undamped propagation. We shall return to this below, but will first specialize (6) to the case of interest in Part I, i.e. perpendicular propagation $(k_\parallel = 0)$. We obtain

$$K(\omega,k_\perp) = 1 - \frac{\omega_p^2}{\omega_c^2} \sum_{n=-\infty}^{\infty} a_n(k_\perp) \frac{n\omega_c}{\omega - n\omega_c} = 0 \ , \qquad (8)$$

$$a_n(k_\perp) = -\frac{\omega_c^2}{k_\perp^2} \int d\underset{\sim}{v} \frac{1}{v_\perp} \frac{\partial f_0}{\partial v_\perp} J_n^2 \left( \frac{k_\perp v_\perp}{\omega_c} \right) \ . \qquad (9)$$

For computational purposes, an integral representation is useful,

$$K(\omega,k_\perp) = 1 + \frac{\omega_p^2}{\omega_c^2} \int_0^\pi d\tau \, \frac{\sin \Omega\tau}{\sin \Omega\pi} \sin \tau \, F_0(\tau + \pi) \quad , \tag{10}$$

$$F_0(\tau) = F_0(\tau + 2\pi) = \int d\underset{\sim}{v} \, f_0(v_\perp, v_\parallel) \, J_0\left(2 \frac{k_\perp v_\perp}{\omega_c} \sin \frac{\tau}{2}\right) \quad , \tag{11}$$

where $\Omega$ has been written for $\omega/\omega_c$. Note that (8) and (10) are analytic over the entire complex $\omega$-plane, except possibly at $\omega = n\omega_c$.

Although detailed numerical studies are generally needed to appreciate the implications of (10), consideration of some simple limiting forms may be helpful. For example, consider the case where $\omega_p^2/\omega_c^2 \ll 1$, and $\omega \approx n\omega_c$. We may approximate the infinite series in (8) by the nth term, so that

$$K(\omega,k_\perp) \approx 1 - \frac{\omega_p^2}{\omega_c^2} a_n(k_\perp) \frac{n\omega_c}{\omega - n\omega_c} = 0 \quad . \tag{12}$$

Solving for the frequency, we find,

$$\omega(k_\perp) \approx n\omega_c \left[1 + \frac{\omega_p^2}{\omega_c^2} a_n(k_\perp)\right] \quad , \tag{13}$$

establishing that there is a mode near each harmonic of the electron cyclotron frequency. It may be shown more generally that there are always cutoffs ($\underset{\sim}{k} = 0$) at $n\omega_c(|n| > 1)$, and the upper hybrid frequency $\left(=(\omega_p^2 + \omega_c^2)^{\frac{1}{2}}\right)$, and resonances ($\underset{\sim}{k} = \infty$) at $n\omega_c(|n| > 0)$. For this reason, the waves are often referred to as 'cyclotron harmonic waves' (CHW). We shall adopt this title in what follows.

## Stability Considerations

Two topological forms of $a_n(k_\perp)$ will be examined in Sections 3-6: first, such that $a_n(k_\perp) > 0$ for all real $k_\perp$, and second, such that it

undulates about the line $a_n(k_\perp) = 0$. Baldwin and Rowlands (1966) have shown that the first case is a sufficient condition for stable CHW propagation. It is satisfied by distributions such as the Maxwellian with $\partial f_0/\partial v_\perp < 0$ $(v_\perp > 0)$. It follows that a necessary condition for instability is that $\partial f_0/\partial v_\perp > 0$ for some range of $v_\perp$.

It will be noted from (13) that if $a_n(k_\perp)$ can undulate, the amplitude of the undulation increases with $\omega_p^2/\omega_c^2$. Consequently, the loops above a given harmonic may ultimately intersect those below the next harmonic. This mode coupling will be shown in Section 3 to produce instability, but it may be appreciated by making a two-term approximation to (8),

$$K(\omega,k_\perp) \approx 1 - \frac{\omega_p^2}{\omega_c^2}\left[\frac{a_n\, n\omega_c}{\omega - n\omega_c} + \frac{a_{n+1}(n+1)\omega_c}{\omega - (n+1)\omega_c}\right] = 0 \quad . \tag{14}$$

This can be rearranged as the quadratic equation,

$$\omega^2 - q_1\omega_c\omega + q_2\omega_c^2 = 0 \quad ,$$

$$q_1 = (2n+1) + \frac{\omega_p^2}{\omega_c^2}\left[n a_n + (n+1)a_{n+1}\right] \quad ,$$

$$q_2 = n(n+1)\left[1 + \frac{\omega_p^2}{\omega_c^2}(a_n + a_{n+1})\right] \quad . \tag{15}$$

Complex solutions, and hence instability, can occur if there are values of $k_\perp$ for which $q_1^2 < 4q_2$. If this turns out to be the case, either within the validity of the approximation leading to (15), or after study of the full dispersion relation, a more detailed examination is required to determine the nature of the instability.

## Instability Classification

CHW are solutions of our basic linearized differential equations, varying as $\exp i(\omega t - \underset{\sim}{k}\cdot\underset{\sim}{r})$, with $\omega$ and $\underset{\sim}{k}$ related via the dispersion

relation $K(\omega,\underset{\sim}{k}) = 0$. If $\underset{\sim}{k}$ is real and $\omega_i < 0$, the wave amplitude will increase exponentially with time for any $\underset{\sim}{r}$, no steady state conditions appear possible. It was pointed out by Sturrock (1958), however, that there are two distinct types of instabilities, one of which does lead to a steady state. The difference becomes apparent only after a spectrum of waves is superimposed by carrying out the inversion described by (7). As $t \to \infty$, (7) may take on one of two forms when instabilities are present: the amplitude of the fluctuating electric field may grow in time at every point in space, or the growing disturbance may propagate away, leaving the plasma in a quiescent condition. The former case is referred to as 'absolute' instability, and the latter as 'convective' instability. The importance of making this distinction should now be clear. If the plasma is convectively unstable, a steady state exists, and it should be possible to excite sinusoidal oscillations, characterized by $\omega$ real and $\underset{\sim}{k}$ complex.

The nature of the instability is determined by the analytic properties of $\underset{\sim}{G}(\omega,\underset{\sim}{r})$ in the lower half complex $\omega$-plane: analyticity there permits convective instability, while a singularity implies absolute instability (Derfler 1961, 1967, 1968; Briggs 1964). The singularities occur at frequencies where the contour of integration (or surface of integration if the integral is multidimensional) of $\underset{\sim}{G}(\omega,\underset{\sim}{r})$ is pinched by zeros of $K(\omega,\underset{\sim}{k})$. For example, for perpendicular propagation as $\exp i(\omega t - k_\perp x)$ we can write,

$$\underset{\sim}{G}(\omega,\underset{\sim}{r}) \equiv \hat{\underset{\sim}{x}}\, G(\omega,x) = \hat{\underset{\sim}{x}} \int_{-\infty}^{\infty} \frac{dk_\perp}{2\pi} \frac{\exp(-ik_\perp x)\rho_s(\omega,k_\perp)}{\epsilon_0 k_\perp K(\omega,k_\perp)} \quad , \qquad (16)$$

where $\hat{\underset{\sim}{x}}$ is a unit vector along the x-axis. Figure 1 shows the contour of integration that uniquely defines $G(\omega,x)$ over the entire complex $\omega$-plane. As $\omega$ moves away from the Laplace contour, it may be necessary to deform the contour into the complex plane to avoid an approaching singularity. This deformation becomes impossible if zeros of $K(\omega,k_\perp)$ pinch the contour as illustrated.

It can be readily demonstrated that at the point of pinching $\partial K/\partial k_\perp = 0$, or equivalently $\partial\omega/\partial k_\perp = 0$, implying that $G(\omega,x)$ has a

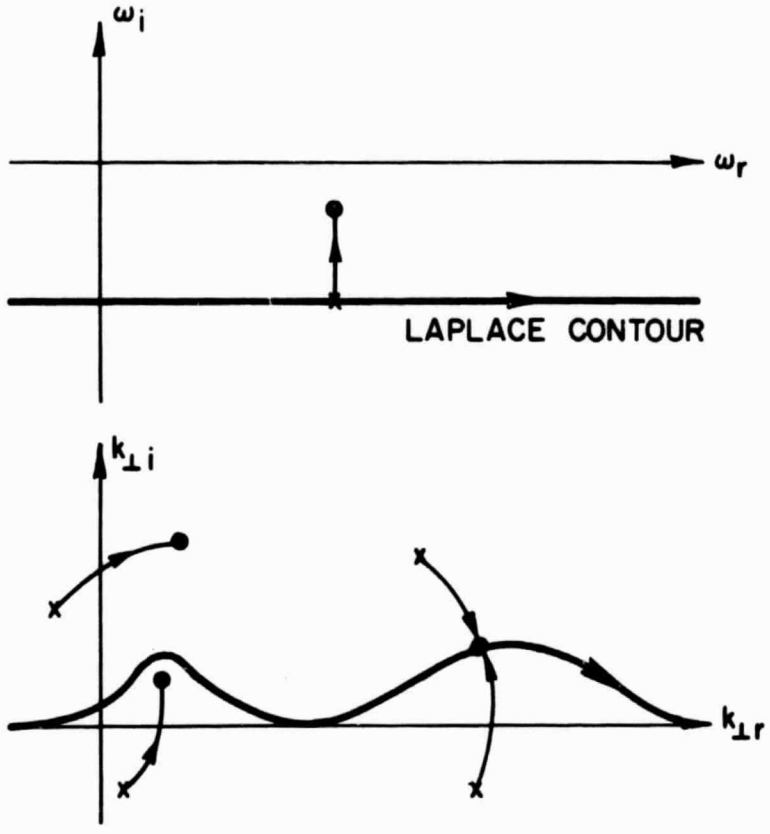


Fig. 1. DEFORMATION OF CONTOUR OF INTEGRATION OF (16) as $\omega$ APPROACHES REAL AXIS FROM THE LAPLACE CONTOUR.

branch point at the same frequency as $k_\perp(\omega)$ has. We may make use of this fact to provide an alternative to the pinching-pole criterion just described. If a mapping of the real $k_\perp$ axis into the complex $\omega$-plane traces a loop located entirely in the lower half of the plane, a branch point of $k_\perp(\omega)$ must be encircled. This implies that $G(\omega,x)$ has a branch point at the same frequency, and hence that the plasma is absolutely unstable. We shall use this later to show that all of the instabilities described in Part I are absolute.

## 3. RING DISTRIBUTION

The ring distribution describes monoenergetic electrons, moving only in the plane perpendicular to the magnetic field, and uniformly distributed in velocity space on a circle with radius $v_{0\perp}$. It may be written in terms of Dirac δ-functions as

$$f_0(v_\perp, v_\parallel) = \frac{1}{2\pi v_{0\perp}} \delta(v_\perp - v_{0\perp})\, \delta(v_\parallel) \quad . \tag{17}$$

With this distribution, integration of (9) and (11) yields

$$a_n(k_\perp) = \frac{1}{\mu_\perp} \frac{dJ_n^2(\mu_\perp)}{d\mu_\perp} \quad , \quad F_0(\tau) = J_0\left(2\mu_\perp \sin\frac{\tau}{2}\right) \quad , \tag{18}$$

where $\mu_\perp = k_\perp v_{0\perp}/\omega_c$. Substitution of (18) in (8) and (11), and some manipulation, gives the following alternative forms for the dispersion relation,

$$K(\omega, k_\perp) = 1 - \frac{\omega_p^2}{\omega_c^2} \sum_{n=-\infty}^{\infty} \frac{1}{\mu_\perp} \frac{dJ_n^2(\mu_\perp)}{d\mu_\perp} \frac{n\omega_c}{\omega - n\omega_c} \quad ,$$

$$= 1 + \frac{\omega_p^2}{\omega_c^2} \int_0^\pi d\tau \, \frac{\sin \Omega\tau}{\sin \Omega\pi} \sin\tau \, J_0\left(2\mu_\perp \cos\frac{\tau}{2}\right) ,$$

$$= 1 - \frac{\omega_p^2}{\omega_c^2} \frac{\Omega\pi}{\sin \Omega\pi} \frac{\partial}{\partial\mu_\perp} \left[J_\Omega(\mu_\perp)\, J_{-\Omega}(\mu_\perp)\right] = 0 \quad . \tag{19}$$

### Dispersion Characteristics

Figure 2 shows numerical solutions to (19) for several values of $\omega_p^2/\omega_c^2$. We note that for $\omega_p^2/\omega_c^2 < 6.62$ the branches undulate about successive cyclotron harmonics. It is easy to see from the final form of (19) that if $\Omega = n$, then $J_n(\mu_\perp)\partial J_n(\mu_\perp)/\partial\mu_\perp = 0$, implying that the modes cut the cyclotron harmonic lines at the zeros of $J_n(\mu_\perp)$ and its

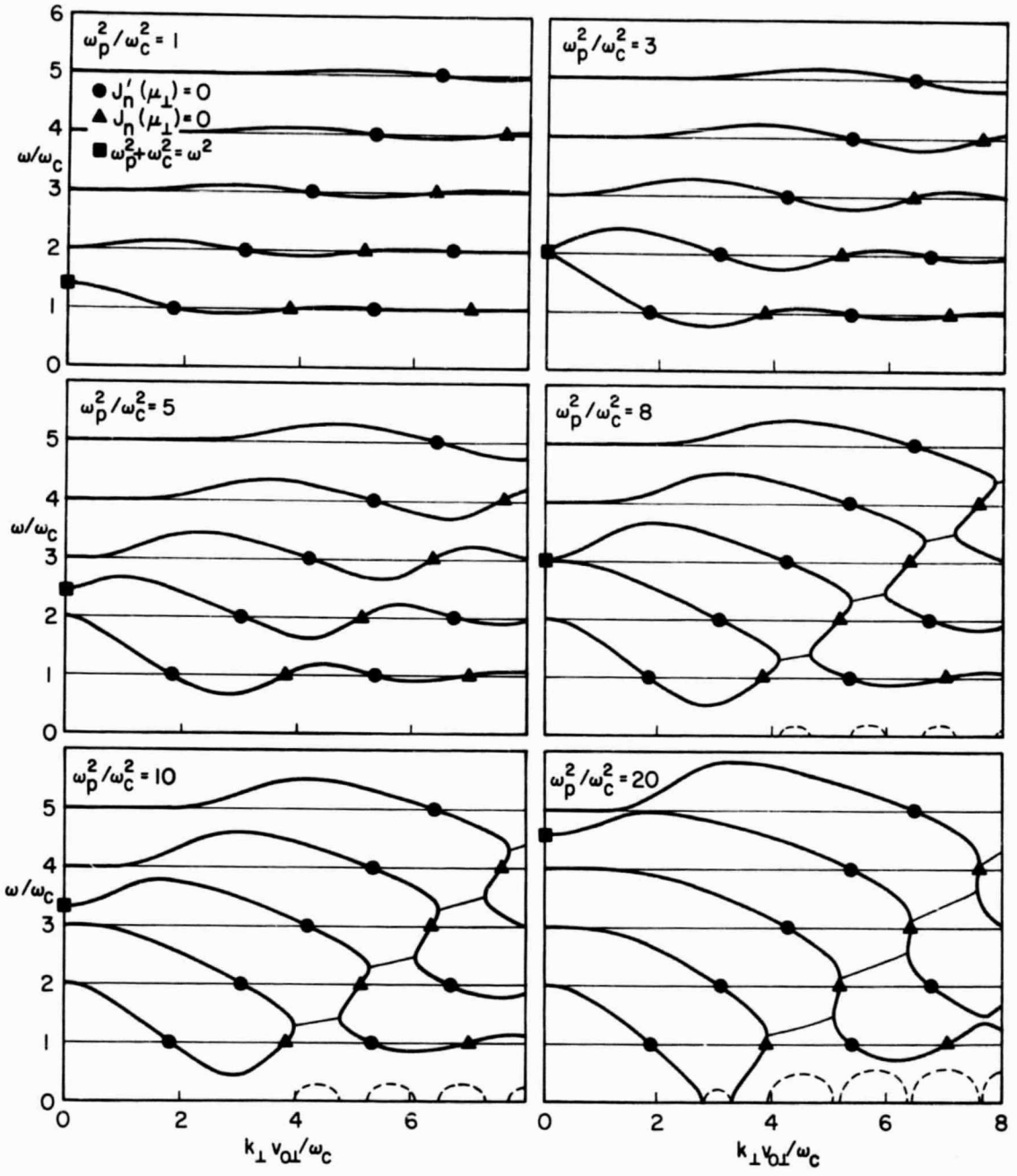


Fig. 2. DISPERSION CHARACTERISTICS OF PERPENDICULARLY PROPAGATING CYCLOTRON HARMONIC WAVES: RING DISTRIBUTION.

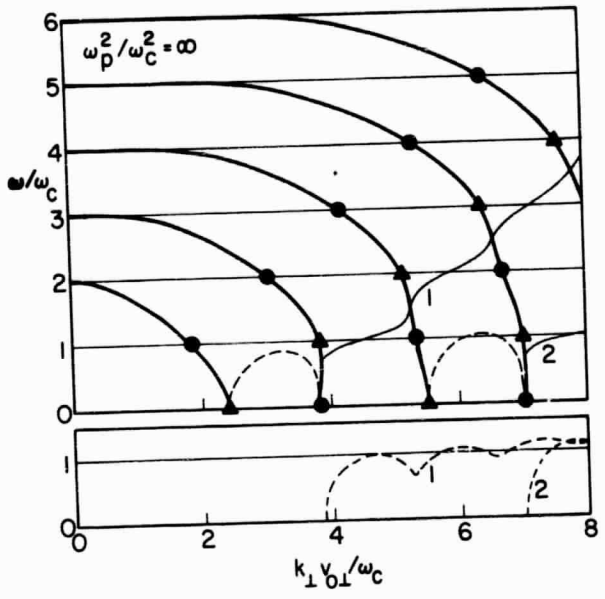


Fig. 2. CONTINUED.

derivative.

As $\omega_p^2/\omega_c^2$ increases, the loops above a given harmonic approach the loops below the harmonic immediately following it. The points at which the loops can couple must always lie between $\alpha_{nm}$ and $\alpha_{(n+1)m}$, where $\alpha_{nm}$ represents the mth zero of $J_n(\mu_\perp)$. The values of $\omega_p^2/\omega_c^2$ at which the first few modes just touch are given in Table 1.

| Distribution | Frequency Band | | | |
|---|---|---|---|---|
| | $0<\omega/\omega_c<1$ | $1<\omega/\omega_c<2$ | $2<\omega/\omega_c<3$ | $3<\omega/\omega_c<4$ |
| Ring | 17.02 | 6.81 | 6.62 | 6.94 |
| Spherical Shell | -- | 215.38 | 57.05 | 47.91 |

TABLE 1. Instability threshold values of $\omega_p^2/\omega_c^2$

After coupling has occurred, there are ranges of $\mu_\perp$ in which purely real solutions for $\omega$ do not exist. The real parts $\omega_r/\omega_c$ of the complex conjugate roots for frequency are indicated in figure 2 by fine lines, and the corresponding imaginary parts $\omega_i/\omega_c$ are shown dotted. Note that these growth rates can become very strong indeed. For example, when $\omega_i/\omega_c \sim 1$, growth rates of the order of 50 dB per cyclotron period $(= 2\pi/\omega_c)$ are implied.

An interesting feature of figure 2 is the occurrence of an instability with $\omega_r/\omega_c = 0$, implying that plasma fluctuations will grow in time without propagation. The threshold conditions for this are obtained by setting $\omega = 0$ in (19), and expressing the result in the form

$$-\frac{1}{2\left(\omega_p^2/\omega_c^2\right)} = \frac{J_0(\mu_\perp)\, J_1(\mu_\perp)}{\mu_\perp} \quad . \tag{20}$$

Since $\mu_\perp$ is real, this equation can be satisfied only if the line $-1/2(\omega_p^2/\omega_c^2)$ lies above a minimum of $J_0(\mu_\perp)\, J_1(\mu_\perp)/\mu_\perp$. When this occurs, there exist purely imaginary roots of the dispersion relation. This can occur only if $\mu_\perp$ lies between succeeding pairs of zeros of $J_0$ and $J_1$.

## Stability Analysis

Since complex $\omega$ solutions occur with $\omega_i < 0$ for $k_\perp$ real, we must apply the instability criteria summarized in Section 2. Figure 3a indicates the use of the pinching pole criterion for the particular case of $\omega_p^2/\omega_c^2 = 20$ and $1 < \omega_r/\omega_c < 2$. When contours A, B, C and D are mapped into the complex $\kappa_\perp$-plane via (19), a saddle point is found at $\mu_{\perp 0} = (k_\perp v_{0\perp}/\omega_c)_0 = 4.46 + i\ 0.18$. The corresponding frequency is $(\omega/\omega_c)_0 = 1.29 - i\ 0.47$. Since the saddle point is formed by the merging of two roots of the dispersion relation that originate on opposite sides of the real axis, and hence the contour of integration, pinching occurs, and $G(\omega,x)$ is singular in the lower half complex $\omega$-plane at $\omega_0$. Hence, the plasma is absolutely unstable.

To illustrate the loop criterion, figure 3b shows the type of locus followed in figure 3a by the complex $\omega$ roots of the CHW dispersion relation as $k_\perp$ increases along the real axis $(k_{\perp i} = 0)$. All the instabilities covered in Part I are of the mode coupling type, and exhibit similar behavior. To separate the two branches in figure 3b, a second locus has been drawn along which $k_{\perp i} = \delta$, where $\delta$ is small and positive. The equation describing this locus is obtainable by expanding the frequency $\omega(k_{\perp r} + i\delta)$, in a Taylor series,

$$\omega(k_{\perp r} + i\delta) \approx \omega(k_{\perp r}) + i\delta \frac{\partial \omega(k_{\perp r})}{\partial k_{\perp r}} \quad , \tag{21}$$

where $\omega(k_{\perp r})$ and the sign of its derivative are evident from dispersion diagrams such as figure 2. A loop in the lower half $\omega$-plane is invariably indicated. This leads to the conclusion that when CHW instabilities occur for perpendicular propagation, they are absolute.

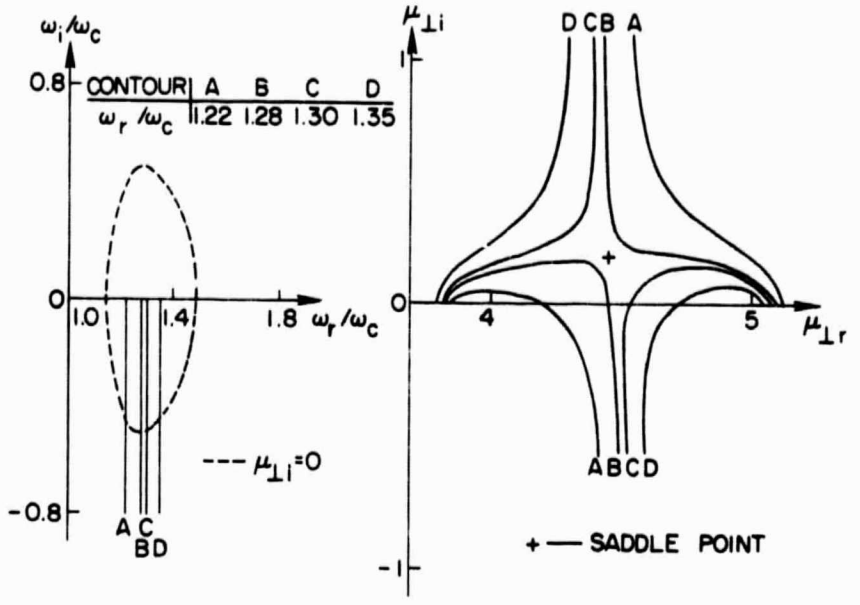


(a) Pinching pole criterion

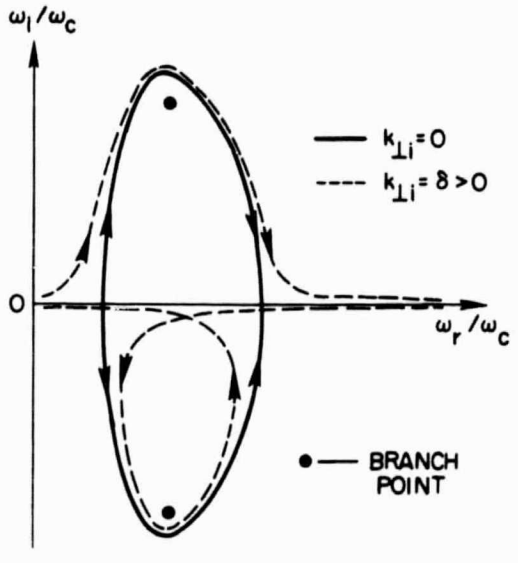


(b) Frequency loop criterion

Fig. 3. APPLICATION OF INSTABILITY CRITERIA TO PERPENDICULARLY PROPAGATING CYCLOTRON HARMONIC WAVES.

## 4. SPHERICAL SHELL DISTRIBUTION

Even if a pure ring distribution could be set up instantaneously, it would diffuse in velocity space due to collisions, and nonlinear wave/particle and wave/wave interactions. In this section, we shall consider as a relevant standard form the spherical shell distribution,

$$f_0(v_\perp, v_\parallel) = \frac{1}{4\pi v_0^2}\,\delta(v - v_0) \quad , \tag{22}$$

where $v = (v_\perp^2 + v_\parallel^2)^{\frac{1}{2}}$. This describes a plasma in which all electrons have the same speed, $v_0$, and are isotropically distributed in velocity space on a sphere of radius $v_0$. The ring distribution would, in principle, relax to this case after the electrons have undergone collisions in which only momentum is transferred. If energy is also transferred during the collisions, the distribution will evolve toward the Maxwellian, which we shall study in Section 5.

With (22), integration of (9) and (11) yields

$$a_n(k_\perp) = \frac{J_{2n}(2\xi_\perp)}{\xi_\perp^2} \quad , \quad F_0(\tau) = \frac{\sin 2\xi_\perp \sin\frac{\tau}{2}}{2\xi_\perp \sin\frac{\tau}{2}} \quad , \tag{23}$$

where $\xi_\perp = k_\perp v_0/\omega_c$. Substitution of (23) in (8) and (11), and use of some Bessel function identities gives the following alternative forms for the dispersion relation.

$$K(\omega, k_\perp) = 1 - \frac{\omega_p^2}{\omega_c^2} \sum_{n=-\infty}^{\infty} \frac{J_{2n}(2\xi_\perp)}{\xi_\perp^2} \frac{n\omega_c}{\omega - n\omega_c} \quad ,$$

$$= 1 + \frac{\omega_p^2}{\omega_c^2} \int_0^\pi d\tau \, \frac{\sin\Omega\tau \sin\frac{\tau}{2} \sin\left(2\xi_\perp \cos\frac{\tau}{2}\right)}{\xi_\perp \sin\Omega\pi} \quad ,$$

$$= 1 + \frac{1}{\xi_\perp^2} \frac{\omega_p^2}{\omega_c^2} \left[1 + 4\left(\frac{\omega^2}{\omega_c^2}\right) S_{-1,2\Omega}(2\xi_\perp)\right] = 0 \quad , \tag{24}$$

where the final form is expressed in terms of Lommel's function,

$$S_{-1,2\Omega}(2\xi_\perp) = \frac{-1}{2\Omega \sin\Omega\pi} \int_0^{\pi/2} d\tau \cos 2\Omega\tau \cos(2\xi_\perp \cos\tau) \quad . \qquad (25)$$

## Dispersion Characteristics

Figure 4 shows numerical solutions of (24) for values of $\omega_p^2/\omega_c^2$ similar to those used for figure 2. The modes cut the cyclotron harmonic lines at the zeros of $J_{2n}(2\xi_\perp)$. This may be seen most easily from (25), in which the integral reduces to $\pi J_{2n}(2\xi_\perp)/2$ at $\Omega = n$. The undulations are less violent, and the instability thresholds may be compared in Table 1 with those for the ring distribution. They are much higher, and we note that no zero-frequency instability occurs. This last point may be proved as follows.

To determine the threshold for instability, we put $\omega = 0$. The first form of (24) then reduces to

$$1 + \frac{\omega_p^2}{\omega_c^2}\left[\frac{1 - J_0(2\xi_\perp)}{\xi_\perp^2}\right] = 0 \quad . \qquad (26)$$

Since the left-hand side of this expression is positive definite for real and nonzero $\xi_\perp$, instability can never set in.

When there is mode coupling and instability in the higher passbands, a similar analysis to that of Section 3 shows the instability to be absolute. The generally weaker growth rates are attributable to the spread in transverse energies associated with the spherical shell distribution.

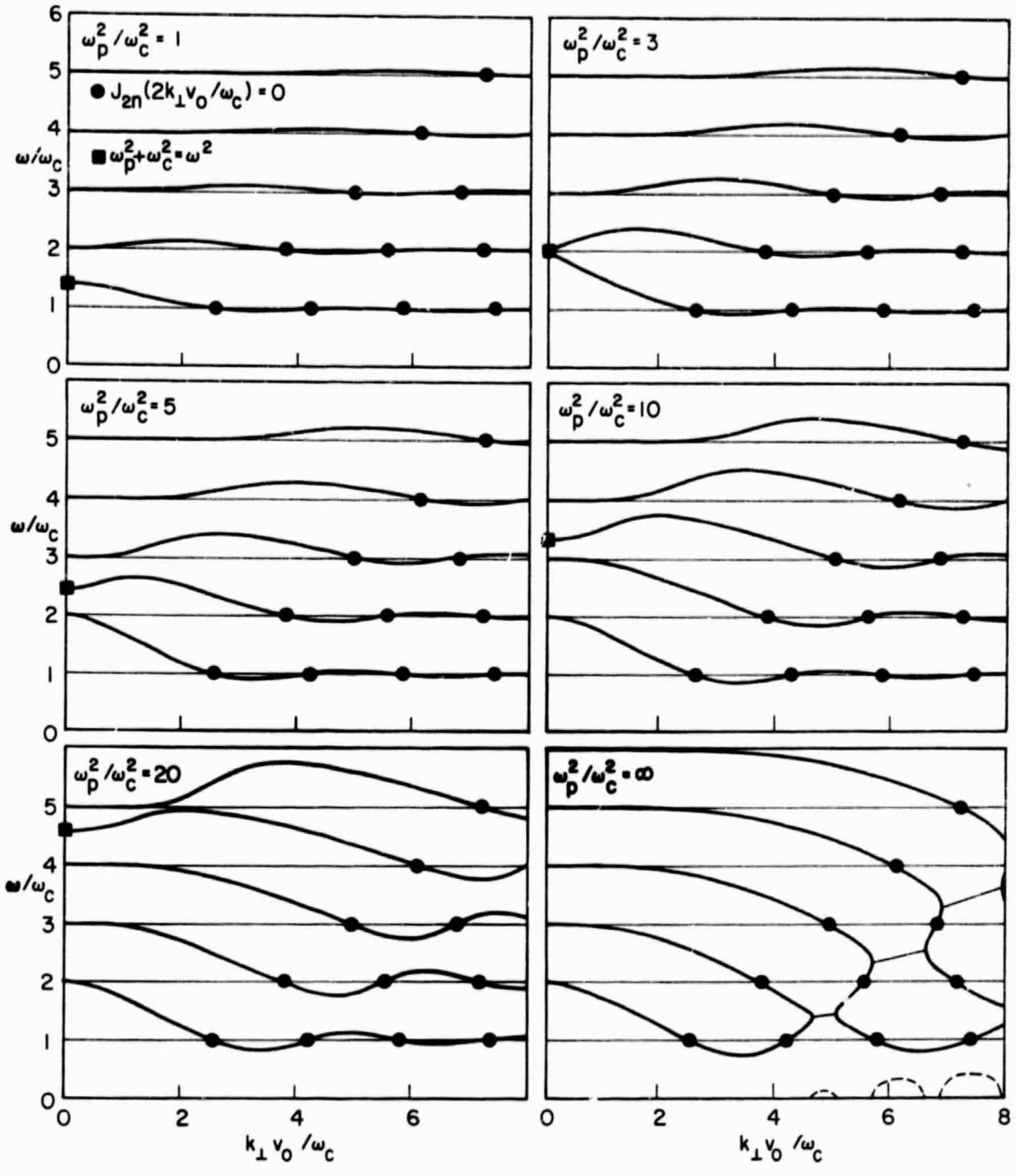


Fig. 4. DISPERSION CHARACTERISTICS OF PERPENDICULARLY PROPAGATING CYCLOTRON HARMONIC WAVES: SPHERICAL SHELL DISTRIBUTION.

## 5. MAXWELLIAN DISTRIBUTION

The final basic distribution to be considered is the Maxwellian,

$$f_0(v_\perp, v_\parallel) = \left(\frac{1}{2\pi v_t^2}\right)^{3/2} \exp\left(-\frac{v_\perp^2 + v_\parallel^2}{2v_t^2}\right) , \qquad (27)$$

where $v_t \left(= (\kappa T_e/m_e)^{\frac{1}{2}}\right)$ is the electron thermal velocity. The now familiar procedure gives

$$a_n(k_\perp) = \frac{\exp(-\lambda) I_n(\lambda)}{\lambda} \quad , \quad F_0(\tau) = \exp\left(-2\lambda \sin^2 \frac{\tau}{2}\right) , \qquad (28)$$

where $\lambda = (k_\perp v_t/\omega_c)^2$. The dispersion relation may be expressed in the alternative forms,

$$K(\omega, k_\perp) = 1 - \frac{\omega_p^2}{\omega_c^2} \sum_{n=-\infty}^{\infty} \frac{\exp(-\lambda) I_n(\lambda)}{\lambda} \frac{n\omega_c}{\omega - n\omega_c} ,$$

$$= 1 + \frac{\omega_p^2}{\omega_c^2} \int_0^\pi d\tau \, \frac{\sin \Omega\pi}{\sin \Omega\pi} \sin\tau \, \exp\left(-2\lambda \cos^2 \frac{\tau}{2}\right) = 0 . \qquad (29)$$

### Dispersion Characteristics

Figure 5 shows numerical solutions $\omega(k_\perp \text{ real})$ of (29) for several values of $\omega_p^2/\omega_c^2$. Since $a_n(k_\perp) > 0$ for all $k_\perp$ real, no mode coupling occurs, and the propagation is stable. Experimental observations of CHW propagation show that these theoretical dispersion characteristics are approached closely in the laboratory (Crawford et al 1967).

Since a Maxwellian plasma is free of absolute instabilities, steady state solutions of (29) can exist for $\omega$ real, and most generally $k_\perp$ complex. Figure 6 illustrates this: In addition to the $\omega$ real, $k_\perp$ real branches already shown in figure 4, there are the $\omega$ real, $k_\perp$ complex branches numbered 1-6. In reality there are an infinite number of them, and a detailed study has been made by Buckley (1968). In general, their

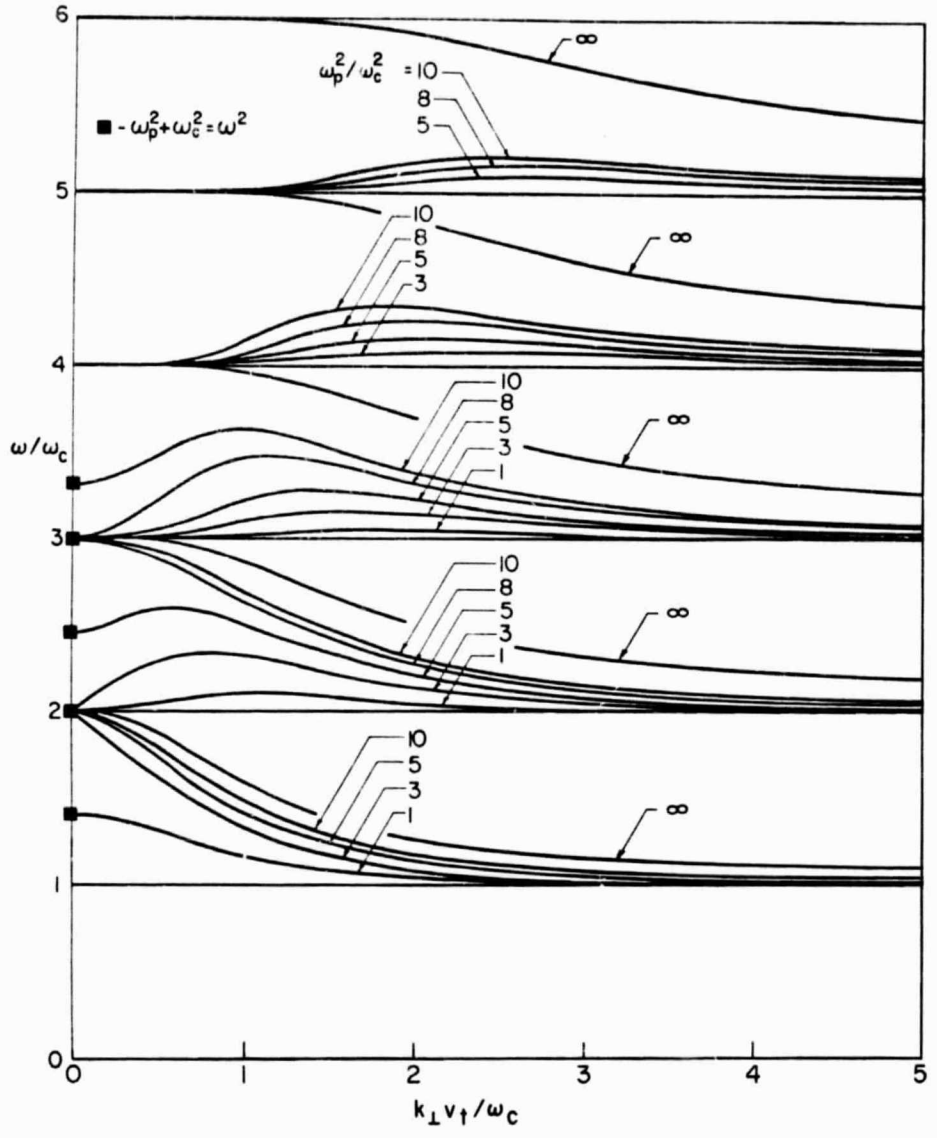


Fig. 5. DISPERSION CHARACTERISTICS OF PERPENDICULARLY PROPAGATING CYCLOTRON HARMONIC WAVES: MAXWELLIAN DISTRIBUTION ($k_\perp$ real).

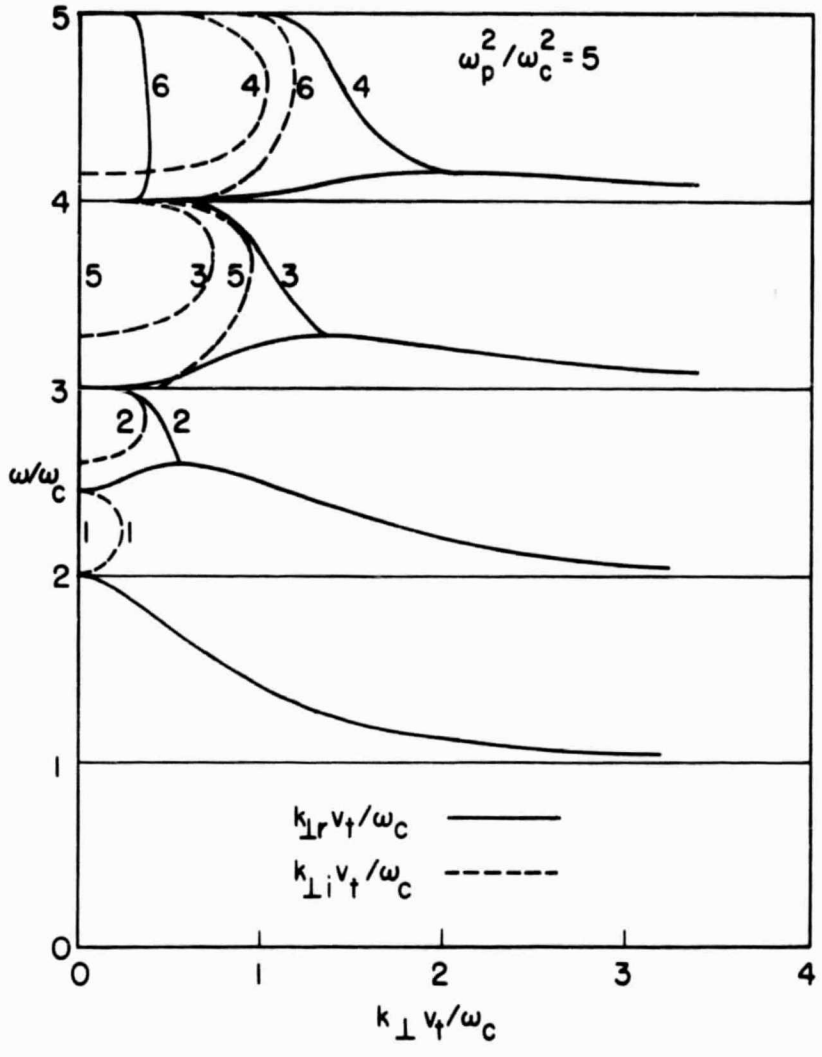


Fig. 6. DISPERSION CHARACTERISTICS OF PERPENDICULARLY PROPAGATING CYCLOTRON HARMONIC WAVES: MAXWELLIAN DISTRIBUTION ($k_\perp$ complex).

spatial decay rates are so high as to make them uninteresting.

These solutions of (29) pose a minor paradox, since they suggest that damped waves can propagate in a lossless plasma. Similar situations occur for other modes of propagation, e.g. surface waves on a bounded plasma column (Ristic et al, 1969), so it is worth pointing out the correct interpretation of this curious result.

Consider (16). If the integration is carried out, defining the contour as in figure 1, we obtain the following representation of $G(\omega,x)$,

$$G(\omega,x) = \sum_n \frac{\exp(-ik_n x)\rho_s(\omega,k_n)}{i\epsilon_0 k_n \partial K(\omega,k_n)/\partial k_\perp} \qquad (x > 0) \quad , \tag{30}$$

where $k_n(\omega)$ is a root of $K(\omega,k_n) = 0$, and the summation extends over all $k_n$ that have a negative imaginary part when $\omega$ is on the Laplace contour. When $\omega$ is real, the terms in this series with complex $k_n$ can be put in pairs, since the symmetry of $K(\omega,k_\perp)$ implies that if $k_n$ is a root with a negative imaginary part, then so is $-k_n^*$, where $^*$ denotes complex conjugate. Thus, the series is constructed of paired expressions

$$\begin{aligned}
&\frac{\exp(-ik_n x)\rho_s(\omega,k_n)}{i\epsilon_0 k_n \partial K(\omega,k_n)/\partial k_\perp} - \frac{\exp(ik_n^* x)\rho_s(\omega,-k_n^*)}{i\epsilon_0 k_n^* \partial K(\omega,-k_n^*)/\partial k_\perp} \\
&\qquad \equiv \frac{\exp(-ik_n x)\rho_s(\omega,k_n)}{i\epsilon_0 k_n \partial K(\omega,k_n)/\partial k_\perp} - \left[\frac{\exp(-ik_n x)\rho_s(\omega,k_n)}{i\epsilon_0 k_n \partial K(\omega,k_n)/\partial k_\perp}\right]^* \\
&\qquad \equiv -2G_{n0}(\omega,k_n)\exp(k_{ni}x)\sin(k_{nr}x-\theta) \quad ,
\end{aligned} \tag{31}$$

where $G_{n0}(\omega,k_n)$ and $\theta$ are defined by,

$$G_{n0}(\omega,k_n)\exp(i\theta) \equiv \frac{\rho_s(\omega,k_n)}{\epsilon_0 k_n \partial K(\omega,k_n)/\partial k_n} \quad , \tag{32}$$

and the source function, $\rho_s(\omega,k_\perp)$, is real and symmetric in $k_\perp$. Since $x > 0$ and $k_{ni} < 0$, the implication of (31) is that the $\omega$ real, $k_\perp$ complex solutions of (29) are associated with the excitation of standing

waves that decay exponentially away from the source. Damped propagating waves will not be excited.

## Collisional Effects

For isotropic distributions such as the Maxwellian, momentum transfer collisions may be taken into account approximately by suitably modifying the dispersion relation. To do so (Tataronis and Crawford, 1965), first replace $\omega$ by $(\omega - j\nu)$, and then $\omega_p^2$ by $\omega_p^2(1 - j\nu/\omega)$, where $\nu$ is the effective momentum transfer collision frequency and is assumed independent of speed. With these substitutions in (29), the four most lightly damped curves of figure 6 become as shown in figure 7. Two quadrants have been drawn for $k_{\perp r} v_t/\omega_c$, to demonstrate clearly how the real parts of the curves join. The imaginary parts indicate strongest damping where the group velocity $(d\omega/dk)$ of the real branches is low or zero for $\nu = 0$. It should be noted that the attenuation is increasingly heavy in the higher passbands, and may easily be of the order of tens of dB/wavelength for the value of $\nu/\omega_c$ chosen.

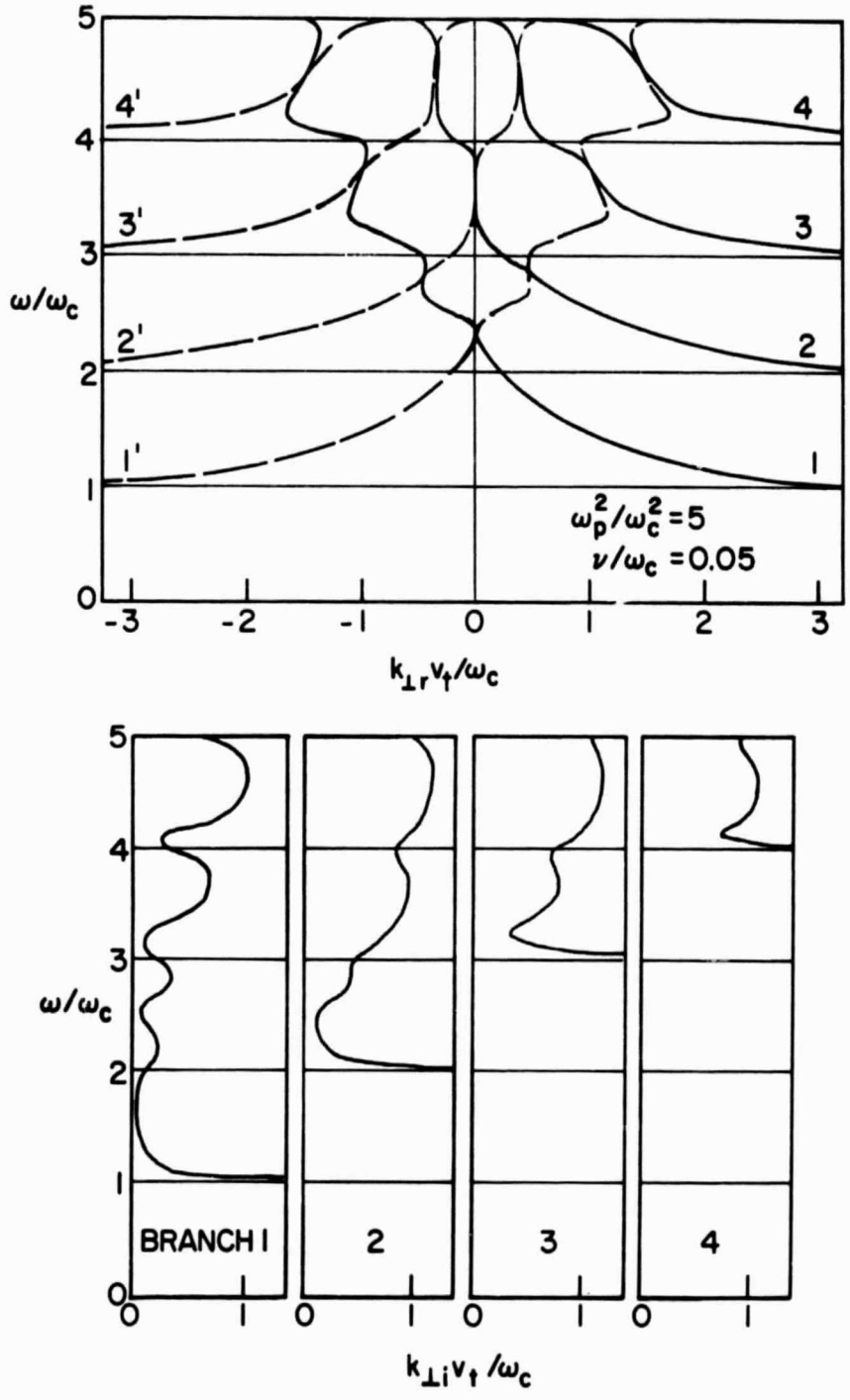


Fig. 7. DISPERSION CHARACTERISTICS OF PERPENDICULARLY PROPAGATING CYCLOTRON HARMONIC WAVES: MAXWELLIAN DISTRIBUTION WITH COLLISIONS.

## 6. MIXED DISTRIBUTION

It is frequently the case experimentally that a group of energetic electrons interacts with a stable background plasma. Since the ring and Maxwellian distributions represent extremes of instability and quiescence, it is natural to investigate a situation in which proportions of these two distributions are mixed. We shall do so in this section with the aims of determining the parameter ranges over which instability will occur, and the strengths and nature of these instabilities. We combine (19) and (29) to obtain

$$K(\omega,k_\perp) = 1 - \frac{\omega_p^2}{\omega_c^2}\left[\alpha \sum_{n=-\infty}^{\infty} \frac{\exp(-\lambda)I_n(\lambda)}{\lambda} \frac{n\omega_c}{\omega - n\omega_c}\right.$$

$$\left. + (1-\alpha) \sum_{n=-\infty}^{\infty} \frac{1}{\mu_\perp} \frac{\partial J_n^2(\mu_\perp)}{\partial \mu_\perp} \frac{n\omega_c}{\omega - n\omega_c}\right] = 0 \quad , \qquad (33)$$

where $\alpha$ defines the proportion of the total electron density that is Maxwellian.

### Dispersion Characteristics

We shall not attempt a detailed review of dispersion characteristics in the $\omega - k_\perp$ form, since we now have not only $\omega_p^2/\omega_c^2$ but also $\alpha$ and $v_{0\perp}/v_t$ as variable parameters. We know the limiting forms for $\alpha = 0$ and 1 (figures 2 and 5), and can deduce that reducing $\alpha$ from unity will cause undulations, due to the ring component $(1-\alpha)$, to appear on the basic Maxwellian curves. The "wavelength" of these undulations along the $k_\perp$ axis will depend on $v_{0\perp}/v_t$. We will return to a specific example shortly, but will investigate first the threshold values of $\omega_p^2/\omega_c^2$ at which mode coupling due to the undulations will occur. Computations based on (33) yield the data shown in figure 8 for the first four passbands.

When $\alpha = 0$ (ring group alone), we retrieve the instability threshold values of table 1. As $\alpha$ increases, the threshold conditions become strongly dependent on $v_{0\perp}/v_t$. In the first passband, $\omega_p^2/\omega_c^2$

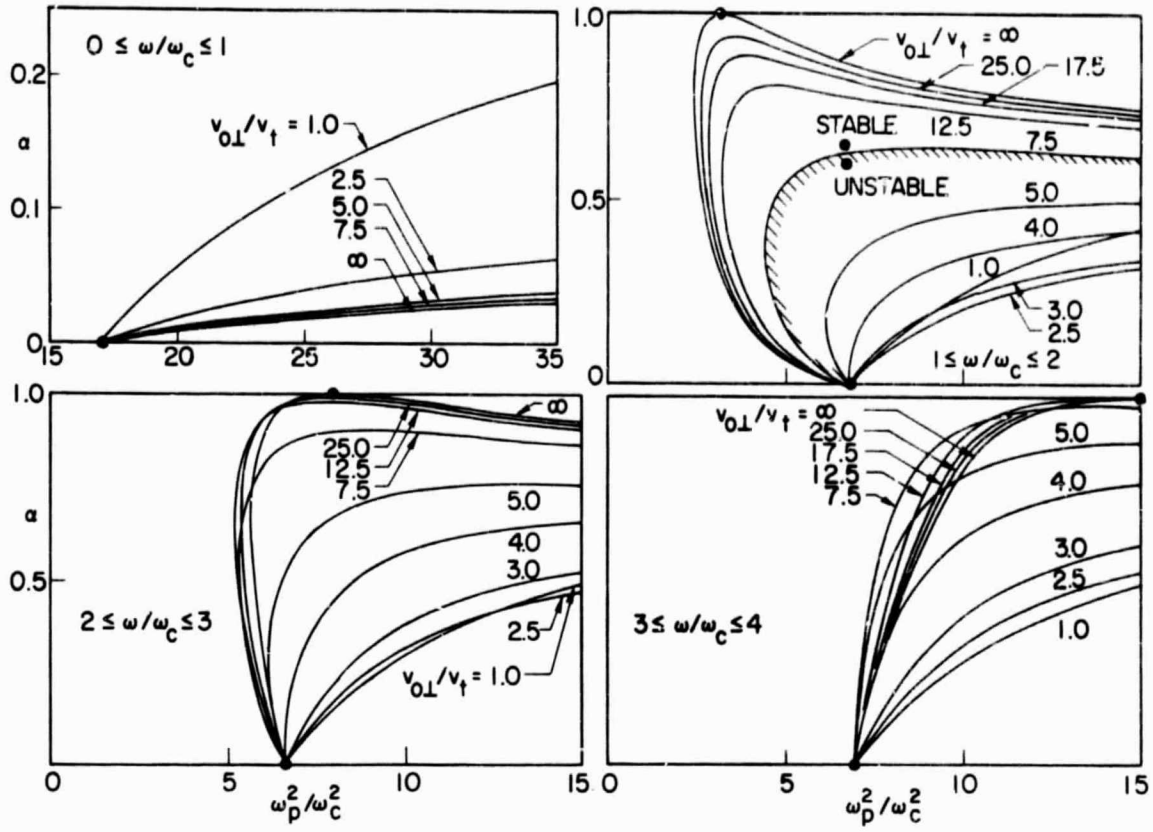


Fig. 8. PERPENDICULARLY PROPAGATING CYCLOTRON HARMONIC WAVES: INSTABILITY THRESHOLD FOR A MIXTURE OF ($\alpha$) MAXWELLIAN AND ($1-\alpha$) RING ELECTRON VELOCITY DISTRIBUTIONS.

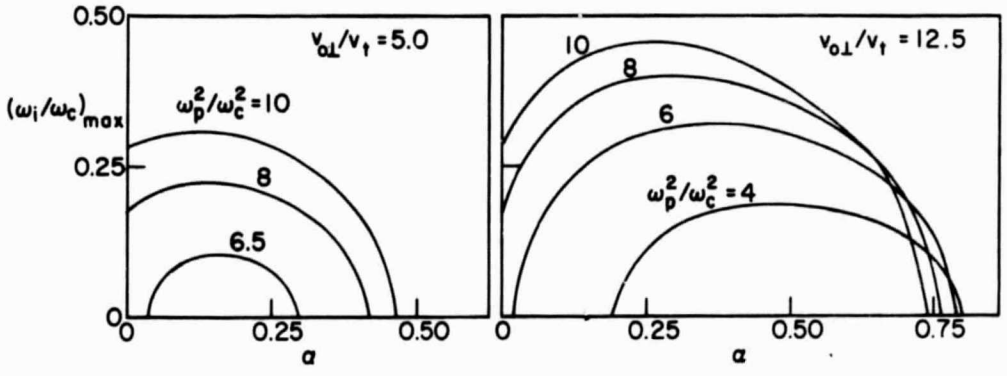


Fig. 9. PERPENDICULARLY PROPAGATING CYCLOTRON HARMONIC WAVES: MAXIMUM INSTABILITY GROWTH RATES FOR A MIXTURE OF ($\alpha$) MAXWELLIAN AND ($1-\alpha$) RING ELECTRON VELOCITY DISTRIBUTIONS.

increases monotonically with $v_{0\perp}/v_t$. The remaining three bands have a more complicated structure, however. For a given $\alpha$, note that the instability threshold may be lowered if $v_{0\perp}/v_t$ is sufficiently large, i.e. instabilities are predicted for values of $\omega_p^2/\omega_c^2$ that correspond to stability when the electrons are exclusively in the ring group. A concomitant of this is that the maximum growth rate associated with the ring distribution alone is increased by addition of some Maxwellian plasma. This is illustrated for the passband $1 \leq \omega_r/\omega_c \leq 2$ in figure 9.

Study of figure 8 indicates that for $v_{0\perp}/v_t \to \infty$ there is instability, even for a vanishingly small population in the ring distribution ($\alpha \to 1$). The threshold values corresponding to this limit are $\omega_p^2/\omega_c^2 = 3$ $(1 \leq \omega/\omega_c \leq 2)$, $8$ $(2 \leq \omega/\omega_c \leq 3)$, $15$ $(3 \leq \omega/\omega_c \leq 4)$, which we recognize as the values for which the upper hybrid frequency equals $n\omega_c$. Near these frequencies, propagating branches of the Maxwellian plasma can easily be coupled together by the undulations caused by the presence of some electrons in a ring distribution. This point is made explicit by figure 10 for the case $\omega_p^2/\omega_c^2 = 3$, $v_{0\perp}/v_t = 25$, which is relevant to the diagram for $1 \leq \omega/\omega_c \leq 2$ in figure 8. As $\alpha$ decreases from 0.96 to 0.90, we see from figure 10 that mode coupling takes place, and there is absolute instability. The growth rate will maximize with decreasing $\alpha$, then decrease again. The final sequence shows how the modes finally become uncoupled as $\alpha$ decreases from $\alpha = 0.40$ to 0.30.

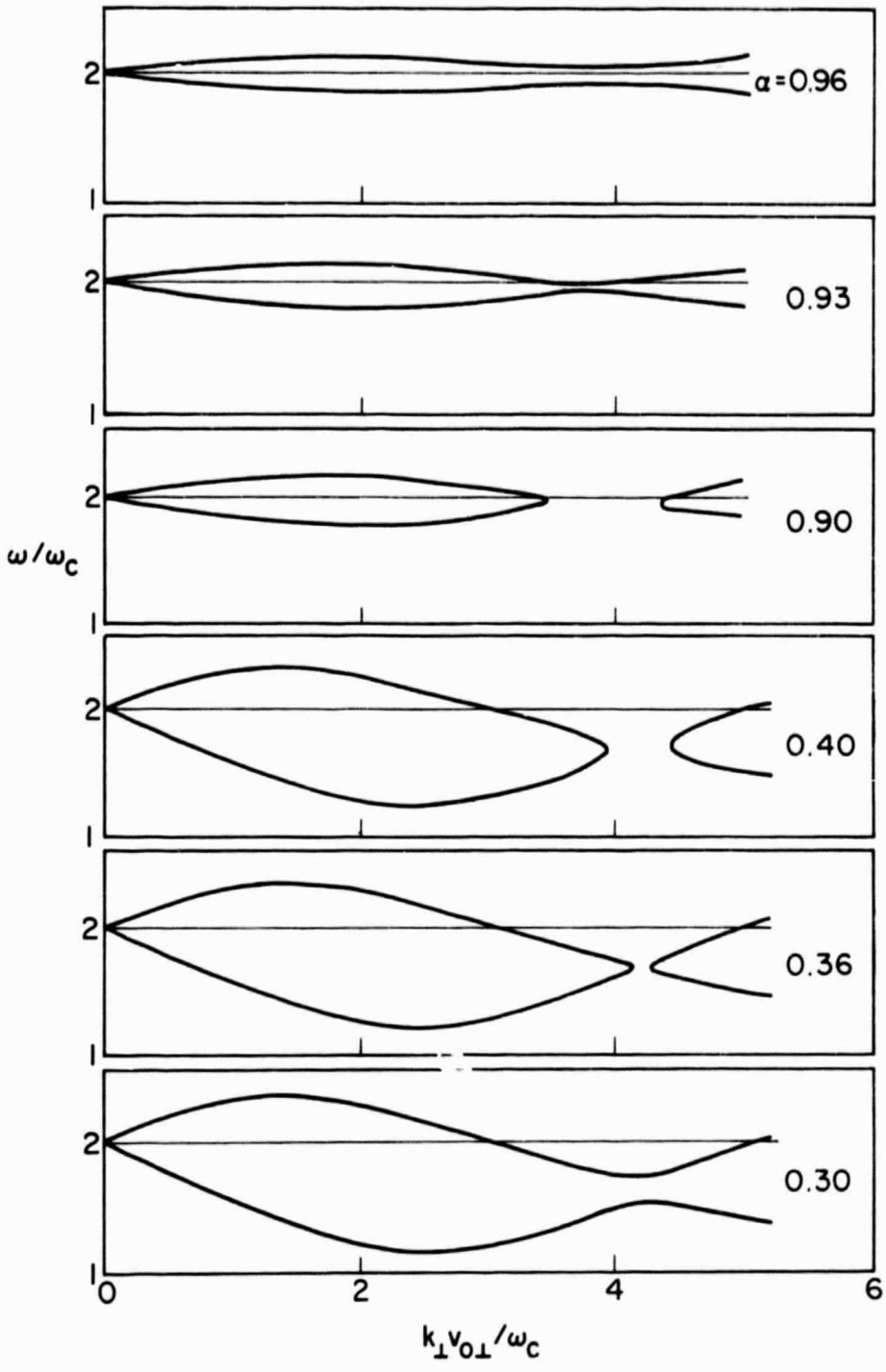


Fig. 10. DISPERSION CHARACTERISTICS OF PERPENDICULARLY PROPAGATING CYCLOTRON HARMONIC WAVES: MIXTURE OF ($\alpha$) MAXWELLIAN AND ($1-\alpha$) RING ELECTRON VELOCITY DISTRIBUTIONS.

## 7. DISCUSSION

In Part I of the paper, we have explored the dispersion characteristics of perpendicularly propagating CHW for a set of basic electron velocity distributions, and it is convenient to summarize here the principal results. The salient features of the ring distribution are its undulatory propagation branches, and the mode coupling leading to very strong absolute instability. The spherical shell distribution shows weaker versions of the same phenomena, but is not subject to a zero-frequency instability. The Maxwellian distribution is associated with stable propagation, and leads to either purely real propagation, or attenuating standing waves. There is no collisionless damping. Finally, our study of a mixture of ring and Maxwellian distributions indicates that the presence of a Maxwellian background may cause absolute instability with higher growth rates, and at lower thresholds $(\omega_p^2/\omega_c^2)$ than for the ring distribution alone.

We may speculate on the results to be obtained for other basic velocity distributions and mixtures. If the shape is given in analytic form, it may be possible to determine immediately from the form of $a_n(k_\perp)$ whether there should be instability or not. If so, its strength might be inferred crudely by considering the transverse velocity spread relative to those of the distributions studied here. It would be academic to push this too far, however, as we shall show in Part II that the instability picture becomes much more complicated when oblique propagation is considered. In particular, growth rates may be higher and instability thresholds lower.

This work was supported by the National Aeronautics and Space Administration, and by the U.S. Atomic Energy Commission. The authors are indebted to Dr. H. Derfler for many helpful discussions.

## REFERENCES


Baldwin, D. E. and Rowlands, G. 1966 Phys. Fluids 9, 2444.

Bernstein, I. B. 1958 Phys. Rev. 109, 10.

Briggs, R. J. 1964 Electron-Stream Interaction with Plasmas. Cambridge, Mass: M.I.T. Press.

Buckley, R. 1968 Proc. NATO Advanced Study Institute on Plasma Waves in Space and in the Laboratory Røros (In press).

Crawford, F. W. 1968 Paper in A Survey of Phenomena in Ionized Gases. Vienna: IAEA.

Crawford, F. W., Harp, R. S., and Mantei, T. D. 1967 J. Geophys. Res. 72, 57.

Crawford, F. W., Lee, J. C., and Tataronis, J. A. 1968 Proc. NATO Advanced Study Institute on Plasma Waves in Space and in the Laboratory Røros (In press).

Derfler, H. 1961 Proc. 5th Int. Conf. Ioniz. Phen. Gases 2, 1423. Amsterdam: North Holland.

Derfler, H. 1967 Phys. Letters 24A, 763.

Derfler, H. 1969 Proc. 9th Int. Conf. Phen. Ioniz. Gases Bucharest (In press).

Stix, T. H. 1962 The Theory of Plasma Waves. New York: McGraw-Hill.

Sturrock, P. A. 1958 Phys. Rev. 112, 1488.

Ristic, V. M., Self, S. A., and Crawford, F. W. 1969 J. Appl. Phys. (In press).

Tataronis, J. A., and Crawford, F. W. 1965 Proc. 7th Int. Conf. Phen. Ioniz. Gases 2, 244. Belgrade: Gradevinska Knjiga.